Journal of Neuroscience Methods 193 (2010) 271–280

Contents lists available at ScienceDirect

Journal of Neuroscience Methods

journal homepage: www.elsevier.com/locate/jneumeth

From spike to graph—A complete automated single-spike analysis

Reut Friedrich*, Uri Ashery**

Department of Neurobiology, The George S. Wise Faculty of Life Sciences, Tel-Aviv University, Tel Aviv, Israel

ARTICLE INFO

Article history:
Received 16 September 2009
Received in revised form 6 September 2010
Accepted 13 September 2010

Keywords:
Amperometry
Chromaffin
Spike
Analysis
SNR
Statistics

ABSTRACT

Amperometry is a commonly used technique for detecting the kinetics of single-vesicle exocytosis with excellent temporal and spatial resolution. However, different methods of analyzing the amperometric signals can produce conflicting conclusions. We developed an efficient automated method for kinetics analysis of single spikes that does not filter the data and therefore prevents distortion of the results. The algorithm assesses the signal-to-noise ratios (SNRs) and accordingly, separates the signals using an adjustable two-threshold calculation. This enables comparing data with different SNRs from different setups. The software also includes a complete statistical analysis, with an automated selection of the most appropriate statistical tests and a graphical representation. The algorithms can be used for any other experimental results requiring the separation of signals from noise, making this method useful for many applications.

1. Introduction

Amperometry, originally developed by Wightman et al. (1991), is a commonly used technique for detecting the kinetics of single-vesicle exocytosis with excellent temporal and spatial resolution. Amperometry provides valuable information on the fine kinetics of transmitter release during vesicular exocytosis and hence has had a great influence on the current view of vesicle exocytosis and the existence of fusion pores (Albillos et al., 1997; Borisovska et al., 2005; Bruns et al., 2000; Jankowski et al., 1993; Mosharov, 2008; Zhang and Jackson, 2008; Zhou et al., 1996). Amperometry detects secreted molecules, usually catecholamine, based on their oxidation at the surface of a small carbon electrode placed near an isolated cell. Such oxidation results in a brief current – the amperometric spike – at the electrode surface (Colliver et al., 2000). Amperometry quantifies the amount and kinetics of releasable cargo from a single vesicle, providing valuable information on single-vesicle fusion dynamics (Amatore et al., 2005; Burgoyne and Barclay, 2002; Elhamdani et al., 2001; Friedrich et al., 2008). Its biggest advantage is that it detects exocytotic events without the confounding effects of concurrent endocytosis (Koh, 2006).

The methods available today for single-spike analysis rely on signal filtering (Gomez et al., 2002; Mosharov, 2008; Mosharov and Sulzer, 2005; Segura et al., 2000). Finding a filter that will reduce noise without distorting some of the main characteristics of the spike, such as amplitude, rising phase and duration, is a very complicated task (Chow and von Rüden, 1995). The most suitable filters for amperometry traces are low-pass filters: these pass low-frequency signals but attenuate signals with frequencies higher than a cut-off frequency. These filters affect mostly high-amplitude spikes and fast spikes (short rising phase). To reduce this problematic effect and to address other problems that occur with filtering (e.g. Gibbs phenomena), several methods have been developed, including the noise-dependent filter (dI/dt) method which chooses the most appropriate filter based on the local noise level (Gomez et al., 2002), or sequential filtering with two different filters (Mosharov, 2008; Mosharov and Sulzer, 2005). Nevertheless, these methods still cause signal distortion. To avoid the complexity of filter selection and importantly, to analyze the signals without the distortion caused by filtering, we sought to develop a method that will use filter only during the detection process and not during the analysis itself.

We developed a novel algorithm that identifies spikes at different signal-to-noise ratios (SNRs), and separates spikes from noise based on their different statistical parameters. This algorithm is a part of automated software that provides a complete solution for single-spike analysis, integration and counting, together with a complete statistical analysis and graphic representation of the results. In the following, we describe the major algorithms comprising our analysis software.

* Department of Neurobiology, Sherman Building Room 712, The George S. Wise Faculty of Life Sciences, Tel-Aviv University, Ramat Aviv, Tel Aviv 69978, Israel. Tel.: +972 3 6408906; fax: +972 3 6407643.
** Department of Neurobiology, Sherman Building Room 719, The George S. Wise Faculty of Life Sciences, Tel-Aviv University, Ramat Aviv, Tel Aviv 69978, Israel. Tel.: +972 3 6409827; fax: +972 3 6407643.
E-mail addresses: reut.friedrich@gmail.com (R. Friedrich), uria@post.tau.ac.il (U. Ashery).
URL: http://www.tau.ac.il/lifesci/neurobiochemistry/faculty/Ashery.htm (U. Ashery).

0165-0270/$ – see front matter © 2010 Elsevier B.V. All rights reserved.
doi:10.1016/j.jneumeth.2010.09.004

2. Methods and results

2.1. Shift correction

An amperometric recording from a cell reveals that the recorded current is the sum of the signal – multiple spikes – and a background-noise signal that oscillates around an average value (the baseline). Different electrodes have different baselines that do not always distribute around zero (Fig. 1A), and the baseline may change during the measurement (Fig. 1A). In addition, the noise's statistical characteristics may change between experiments and could be any combination of noise (pink noise, white noise or other; Fig. 1B), depending on the electrical grounding and shielding in the measuring setup. The "shift correction" operation is highly important as it normalizes the noise within and between measurements and performs this task under any noise combination. By normalizing the noise throughout the entire experiment to fluctuate around the same value ($\mu \approx 0$), our spike identification can use the entire sample for the signal identification constants, making these constants both sensitive and robust. Although the shift-corrected noise ($\mu \approx 0$) and white noise ($\mu = 0$) are very similar, application of a Kolmogorov–Smirnov test revealed that statistically, they are different ($p < 0.001$). Yet the normal model proved to be robust enough to encompass such small deviations. Therefore, the analysis constants used for signal identification, when calculated from the shift-corrected noise, are good representatives of the noise, as demonstrated by our spike-identification abilities.

The method we applied for shift correction starts by removing the outliers in the recording. This is performed by taking a high percentile value (e.g. 99.4%) which insures that the spike's climaxes are left out and thus setting the outliers as the threshold. Namely, on the original recording x, if a value x_i is bigger than the high percentile, then it equals the high percentile ($x_i > P_{\text{high}}$ then $x_i = P_{\text{high}}$). This new cut-off vector does not include any extreme values and in particular, no longer includes the spike's climax.

We then calculate an averages-vector, by calculating the moving average over 21,000 points. Since the average-vector is calculated from such a large window (around 2 s for a 10 kHz sampling rate), both the noise and the signal are averaged out and mainly the recording's base-line is left. Finally, we subtract this vector from the original signal to get the shift-corrected signal: $x_{\text{shift corrected}} = x -$

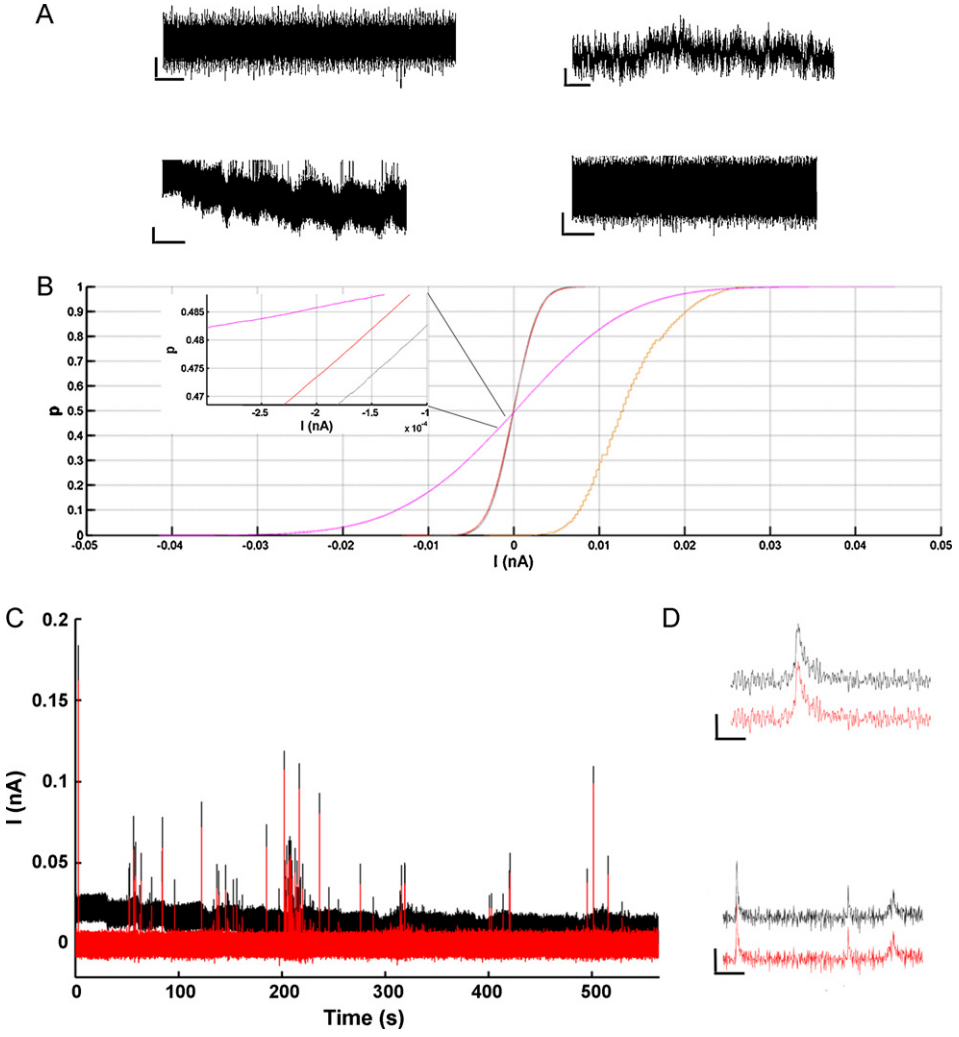

Fig. 1. Noise in amperometry recordings. (A) Upper left: simulation of white noise (bar 5 pA, 70 s). Lower left: amperometric recording demonstrating the noise value of a cell (bar 5 pA, 70 s). Upper right: simulation of pink noise (bar 20 pA, 90 s). Lower right: noise value after shift-correction operation of the amperometric current (bar 5 pA, 90 s). (B) Cumulative density function (CDF) of amperometric noise (brown), pink noise (pink), white noise (gray) and shift-corrected noise (red). Enlargement (inset) shows that the CDF of the shift-corrected noise is between the pink noise CDF and white noise CDF and although the measurement noise is closer to the white noise distribution, it is statistically different from it (see text for details). (C) Demonstration of the shift-correction operation: red trace represents the shift-corrected signal; black trace represents the original signal. (D) Zooming in on the trace demonstrates that the shift-correction action does not harm the signal (bar 10 pA, 1 ms). (For interpretation of the references to color in this figure legend, the reader is referred to the web version of the article.)

Fig. 2. Flow chart of the "find spikes" algorithm. This stage is fully automated. See text for details.

$\bar{x}$. Fig. 1C depicts the shift-correction operation (red trace = shift-corrected signal, black trace = original signal).

2.2. Spike identification

The main steps of the spike-identification algorithm are summarized in the flow chart in Fig. 2. Following shift correction, the algorithm identifies the spikes. For most of them, identifying the peak is usually straightforward since the spike's amplitude is several-fold higher than any measured threshold. However, identifying the spike's edges is more complicated as the signal might be buried in the noise. Nevertheless, extracting this information accurately is important because the edges are relevant in single-spike analyses: the beginning (the foot) represents the opening of the fusion pore, and the exponential decay represents its closure or dispersion of the catecholamine content (Chow and von Rüden, 1995). Therefore, we developed an adjustable two-threshold algorithm: signals above a high threshold are identified as spikes while the low threshold is used to identify the edges of each spike. These thresholds are dynamically calculated based on the SNR level of the recording (see Supplemental methods). Nevertheless, we found that for a wide range of SNRs, these parameters were the same. First, the algorithm calculates a basic threshold where it adds 2.5 s.d. to the data's mean value. Then it separates the data into two groups: values which are larger ("signal") and smaller ("noise") than the basic threshold. This separation is then used for the SNR calculation; the SNR value determines the constants used for calculations of the two refined thresholds (see Supplemental methods).

An example of a spike's identification is illustrated in Fig. 3A. The dark green line represents the high threshold and the light green line, the low threshold. In the next step, the algorithm goes through the vector data and identifies the spikes' start points. A start point is the first data point below the high threshold (Fig. 3B, purple dot). Next it identifies the end points—the last data point above the high

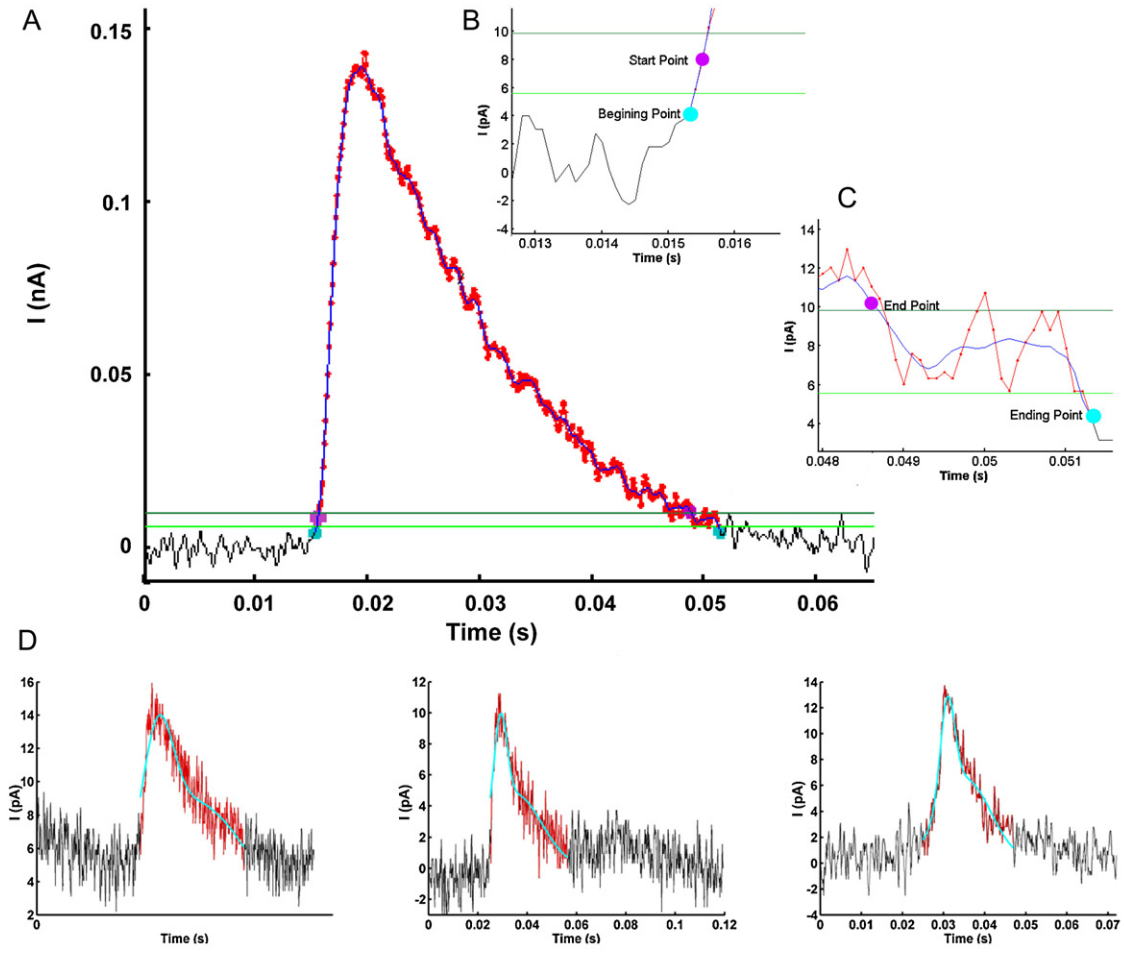

Fig. 3. Illustration of the "find spikes" algorithm. (A) Original amperometric trace (black). Red dots indicate identified spike. (B and C) Enlargement of spike's edge during the identification process. Blue line indicates smoothed signal. Dark green line indicates high threshold, light green line indicates low threshold. Turquoise dots represent the beginning and ending points. Purple dots represent the start and end points. (D) Three small unfiltered spikes with their double-Gaussian fittings. R^2 values of the Gaussian fitting to the spike from left to right are, respectively, 0.81, 0.84, 0.9. (For interpretation of the references to color in this figure legend, the reader is referred to the web version of the article.)

threshold (Fig. 3C, purple dot). Each spike candidate is now represented as the set of points between its start point and end point. This initial identification step is performed on a filtered signal (moving average where number of points is SNR-dependent) to avoid crossing the high threshold due to temporal noise. Note that filtering is only used as an intermediate step to find spike candidates and the spike's parameters are derived from unfiltered signal. The algorithm iterates one spike at a time, to find where the spike begins and where it ends. All subsequent steps are performed with the unfiltered signal.

For edge identification, the algorithm uses the low threshold as a screening parameter in the surrounding area of the start/end points. The algorithm finds the first point before the start point that is below the low threshold: this point is the beginning point of the spike (Fig. 3B, turquoise dot). The ending point of the spike (Fig. 3C, turquoise dot) is the first point after the end point that is below the low threshold. The whole spike is now defined from its beginning point to its ending point.

Although the previous steps were threshold-based, high noise levels were sometimes also classified as small spikes. One possible solution could be to increase the threshold. The downside of this approach is that we would lose many of the small spikes that are just slightly above noise level and might represent the release of catecholamine from a flickering fusion pore. Reviewing the noises that were identified as spikes, we found that they can easily be disqualified with the naked eye based on shape. Using trial and error, we found that the small-amplitude spikes can be well fitted with a double-Gaussian model. Therefore, we implemented an algorithm that would iterate on the small-amplitude spikes and check their fit to the double-Gaussian model. This equation gives a fairly good representation ($R^2 > 0.8$) of the spike's contour, thus enabling to set a shape criterion. Fig. 3D demonstrates several small spikes with their double-Gaussian fitting.

2.3. Comparison to existing methods

The two leading methods for spike identification are filtering and taking a time derivative of the signal. The task of finding a filter that will reduce the noise without distorting the main parameters of the signal has proven to be complicated (Chow and von

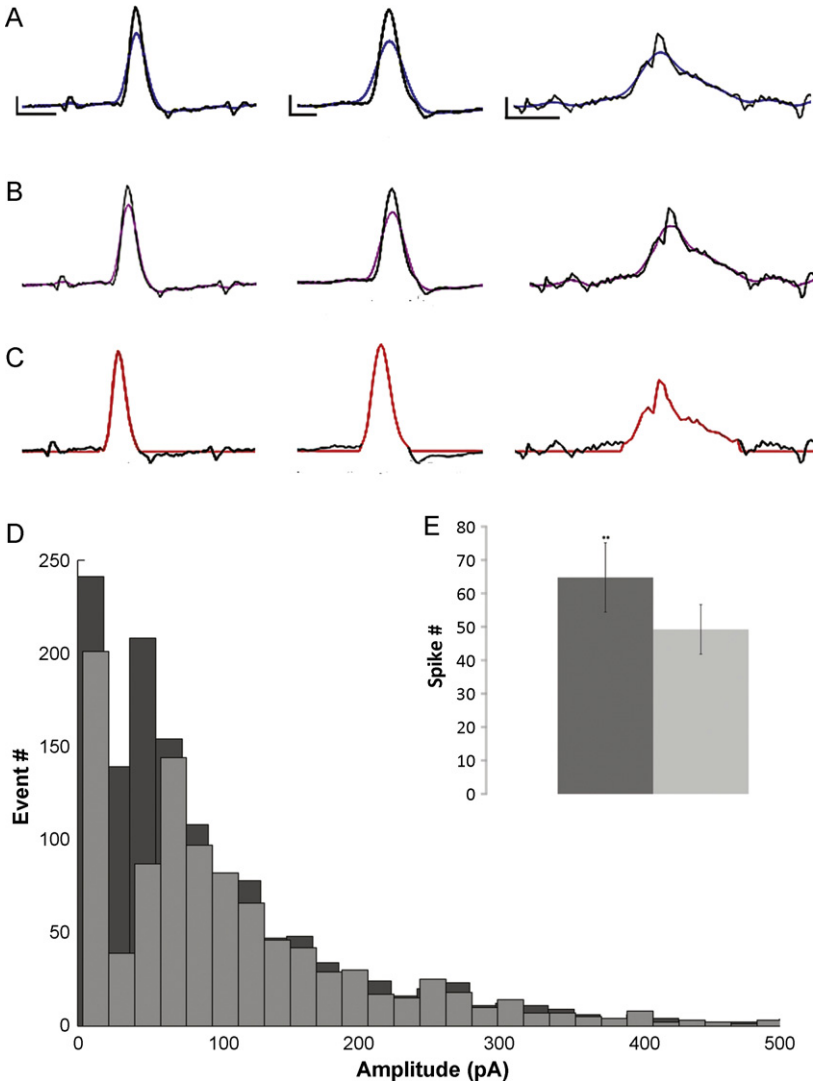

Fig. 4. Comparison of different filtration methods. (A–C) Example spikes filtered with either moving average (10 points) filter (A, in blue) or with Gaussian FIR filter (B, in purple), or NOT filtered but the spikes are identified using the presented method (C, in red), demonstrating the effects of filtration on spikes. Filtering causes a decrease in amplitude, deceleration of the linear phase and shape distortion. Compare to the identification of the same spikes without filtration in the bottom panel. Bars: (left) 5 ms–100 pA, (middle) 2 ms–100 pA, (right) 2 ms–50 pA. (D) Histogram of spike amplitude identified using AmperoStat method (light gray,(Hof, 2003)) and our method (dark gray). (E) Bar plot of the averaged spike number identified by both methods: 64.8 ± 10.4 (our method, dark gray) 49.2 ± 7.3 (Amperostat, light gray), paired Student's *t*-test $p < 0.003$. (For interpretation of the references to color in this figure legend, the reader is referred to the web version of the article.)

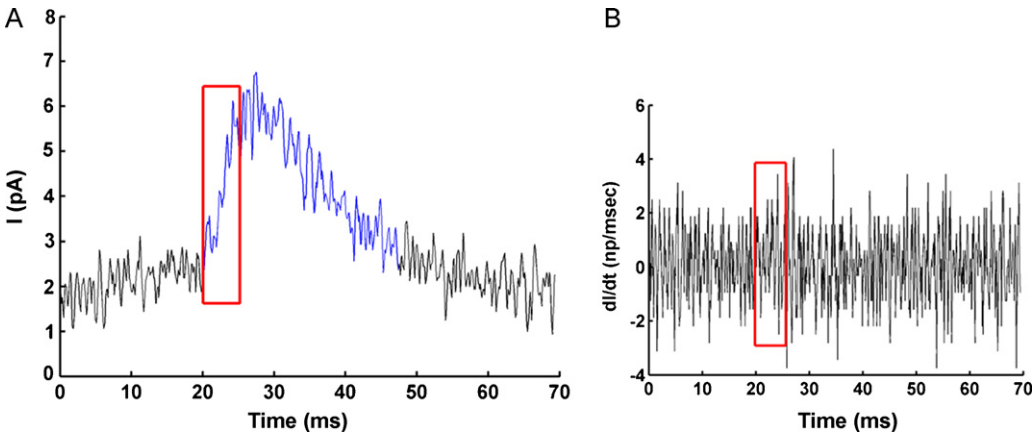

Fig. 5. Identification of small, slow spike. (A) The original trace is presented in black and the identified spike, using our method, is plotted in blue. Red rectangle indicates the rising phase of the spike. (B) First derivative of the trace could not identify this spike. Red rectangle is depicted around the area corresponding to the red rectangle in (A). (For interpretation of the references to color in this figure legend, the reader is referred to the web version of the article.)

Rüden, 1995). The filters commonly used for filtration are low-pass filters, which affect mostly high spikes. Fig. 4A and B demonstrates two described of these low-pass filters: moving average (Marom et al., 2007, 2010; Yizhar et al., 2004) and Gaussian finite impulse response (FIR) (Mosharov, 2008), compared with our method which does not filter the signal (Fig. 4C). As demonstrated in Fig. 4, a filter that may fit one signal well can alter the rising phase, reduce the amplitude and distort the shape of another spike. A method for selecting a cut-off frequency that will not affect the rising phase of the signals is described in (Mosharov, 2008; Mosharov and Sulzer, 2005). In this method, the frequency of the fastest signal is used as the cut-off. A problem with this approach is that such a filter may leave too much noise, especially on small signals: the small and slow signals are ignored, whereas in our experiment, we attempted to analyze them as well, and we were not able to find any filter that could increase the SNR to a level that allows analyzing such signals. Another problem with this method is that the calculation of the cut-off filter requires that the signals already be identified. However, finding the signals is part of the challenge.

A method to address this issue was introduced in (Gomez et al., 2002). Their approach uses the best-fitting filter for each signal but changes the cut-off frequency based on the rising phase of the specific signal being analyzed. Like the previous method, in this method the signal also needs to be identified prior to filtering, while part of the challenge is to identify the signal within the noise. Another potential problem is that by changing the filter for every signal, different distortions are induced on different signals. Namely, a fast signal may need a higher frequency cut-off and thus will exhibit more "noise energy" than a slower signal. In addition, calculating the highest frequency of the rising phase is more complex for slow or small signals where within that phase, there are also noise-related oscillations. In such signals, the maximum frequency during the rising phase could be noise-related and not the frequency of the signal's rising phase. Finally, the noise generally has the same statistical characteristics and frequencies throughout the experiment while the signal behaviors vary. Therefore, it is somewhat counter-intuitive to assume that the noise (constant component) will be filtered out using parameters that are calculated from the signal (changing component).

We compared the ability of our method to identify amperometric signals to that of the AmperoStat macro (Hof, 2003) which is widely used (Marom et al., 2007, 2010) and found that our method identified and analyzed 20% more spikes events especially in non-ideal cells with low SNR and baseline change within the experiment (64.8 ± 10.4 vs. 49.2 ± 7.3, paired Student's t-test $p < 0.003$, Fig. 4E). Plotting the amplitude of the total population of spikes identified by both methods demonstrates the good ability of our method to identify small spikes together with larger ones (Fig. 4D) without affecting the final result by filtering.

One of the advantages of the presented method is that it can even identify slow spikes. The two previous methods use first derivatives to identify the signals. They assume that the first derivative will reach its maximal value during the rising phase of the signal, shortly before the signal reaches its maximal value. We compared the ability of the first-derivative method to the present method and found that whereas slow signals are easily recognized using the presented method, the derivative option was not able to identify small or slow signals (Fig. 5).

2.4. Single-spike parameters

After identifying the spikes, the algorithm iterates on the signal list and calculates each spike's parameters (Fig. 6). The "single-spike parameters" analysis includes the following (Mosharov, 2008; Mosharov and Sulzer, 2005): spike duration (ms), charge (pC), half width ($t_{1/2}$), and amplitude (I_{max}), peak-to-peak time (t_{ptp}) and time of spike climax (T_{max}). Next, the algorithm identifies the linear phase of the spike and fits a linear equation to it. A common method for finding the rising phase relies on fixed numbers (Mosharov and Sulzer, 2005) e.g. 30–70% of the spike's climax (Chow and von Rüden, 1995). The fixed-number method is very convenient for adjusting a linear equation to the data, but it has no biological meaning. We implemented a method that is able to identify the complete rising phase of a spike, i.e. identify consecutive increases in the spike's rising phase (as described further on) that can be fitted with a linear equation with a goodness of fit of over 0.95. Fig. 6B depicts three different lines that the algorithm tries to fit: the blue line is the final line presented in Fig. 6A, and the turquoise line is the fitting of 35–65% of the signal as described in (Fulop and Smith, 2007) which actually has an R^2 of less than 0.95. The difference in the values of the rising-phase parameters might be small between the two methods (our software includes analysis by both methods: ours and 30–70% to enable comparison), yet ours does not rely on convenient and arbitrary selection. Fig. 6 demonstrates the identification of the rising phase and the duration of the linear phase (t_{rise}). Although the algorithm can always identify the spike's rising phase, it cannot always fit a linear equation with R^2 greater than 0.95; in this case, it fits a linear equation to the identified rising phase and returns the parameters. The user can either accept its fit or overwrite it with a manual fit.

Small noisy spikes or flickering foots may not be competent for full analysis. We therefore created a "small event" option in our

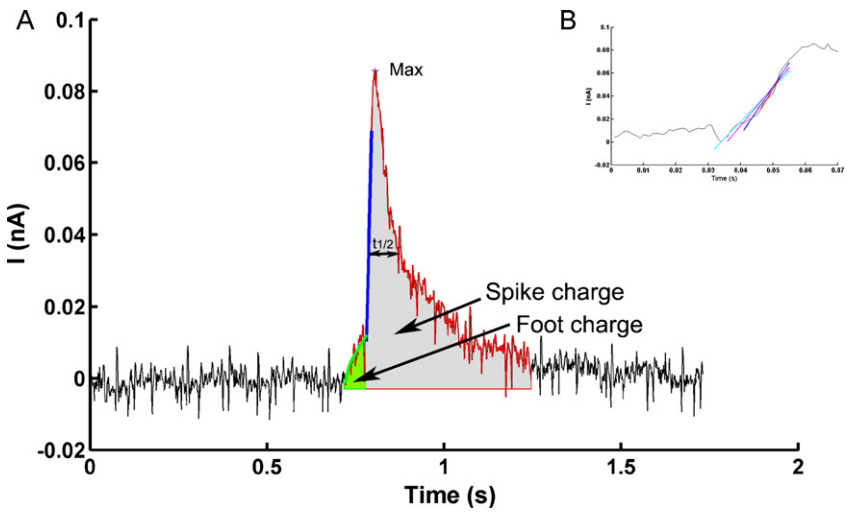

Fig. 6. Representative spike with its analyzed parameters. (A) Original trace illustrated in black, identified spike in red. Blue line represents the rising phase, green line represents the foot. Purple cross represents the spike's amplitude. Gray area is the spike's charge, green area is the foot's charge. (B) Demonstration of the fitting process of the linear model to the rising phase: turquoise line $R^2 = 0.9138$, pink line $R^2 = 0.9334$, blue line $R^2 = 0.9598$ and red is the fitting of the linear equation to 35–65% with $R^2 = 0.9257$. (For interpretation of the references to color in this figure legend, the reader is referred to the web version of the article.)

analysis, where small events are numbered and their basic parameters are calculated (amplitude, charge and duration). The researcher can choose to analyze these events and to calculate their relative contribution to the whole secretion event or to omit them from the analysis.

2.5. Separation of two overlapping spikes

To identify overlapping spikes, we start by identifying the rising phases of each identified spike as already described. First, we slightly smooth the signal to avoid fast noise fluctuations, which can be identified as a double-peak spike. Then we identify the rising phases by number of consecutive points that are on a monotonically increasing line. Each rising phase is a candidate for the beginning of a new signal. However, further criteria have to be met for a peak to be identified as a spike: first, the length of the rise has to be at least n consecutive increases (n is a function of the sampling frequency, e.g. $f = 10$ kHz $n = 5$); spikes with shorter rising phases are discarded as noise. Second, the rise phase amplitude of the smaller spike (Fig. 7, R1 and R2) must be at least 20% of the maximum rise phase amplitude of the larger spike (in Fig. 7: $R2 \geq 20\% \times R1$), and the maxima (end of rising phase minus the global minima, Fig. 7, H1 and H2) must be at least 40% of the highest maximum (in Fig. 7: $H2 \geq 40\% \times H1$). Moreover, the minimum (beginning of rising phase, L2) has to be below 50% of the global maximum (in Fig. 7: $L2 \leq 50\% \times H1$). When all conditions are met, the split candidate is qualified and the split point is the minimal value between the two maxima as depicted in Fig. 7.

2.6. Identifying the foot

Around 30% of exocytotic events recorded by carbon fiber amperometry exhibit a pre-spike feature referred to as a "foot" (Amatore et al., 2009). The foot is associated with the release of neurotransmitters via a transitory fusion pore, whereas the large, main exocytotic spike is due to complete release (Amatore et al., 2009). The algorithm determines the foot parameters after identifying the linear phase. Since not all spikes have a foot, the algorithm should be able to (a) determine whether the spike has a foot and (b) find the foot parameters. The algorithm looks for a foot from the beginning point of the spike until the first point of the linear phase. If the alleged foot is less than 1 ms, it is not considered a foot; otherwise, the algorithm defines the foot parameters using specific fitting algorithms (see below). The fit is plotted as a green line in Fig. 6. For spikes that have a foot, the algorithm calculates the foot's duration, charge and amplitude (A_0 as calculated from the equation).

Spikes with a foot can be divided into two primary categories, depending on the temporal variation of the foot shape (a ramp, or a ramp followed by a plateau) (Amatore et al., 2009). Therefore, we changed the exponential equation suggested for foot description (Chow and von Rüden, 1995) to a combined sigmoid:

$$F(x) = \frac{A}{1 + e^{-\tau(x-x_0)}} + B(x - x_1) + C$$

For a full sigmoid foot, coefficient B will be zero while A will get a non-zero value. For a fully linear foot, coefficient A will be zero while B will be non-zero. Indeed, analysis of several hundred feet demonstrated that we receive the best fit using a combination of the two.

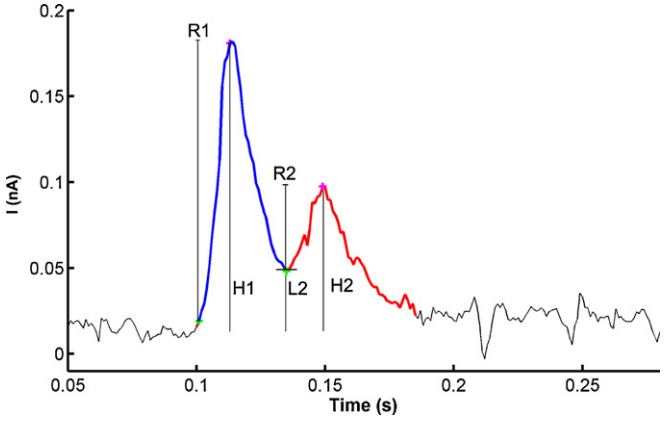

Fig. 7. Separation of overlapping spikes. Identification of overlapping spike—blue color outlines the first spike and red color outlines the second spike. Green + marks the beginning of the rising phase and purple + marks the end of the rising phase. R1, rising phase of signal 1. R2, rising phase of signal 2. H1, amplitude of signal 1. H2, amplitude of signal 2. L2, minimum between the two rising phases ($H2 = L2 + R2$). (For interpretation of the references to color in this figure legend, the reader is referred to the web version of the article.)

2.7. Statistical guideline for single-spike analysis

Proper statistical tests are necessary for correct interpretation of the data. However, the use of specific statistical tests depends on model assumptions, such as data distribution and variance homogeneity. Hence, the experimenter has to decide on the most appropriate statistical test for each data set. We implemented a built-in algorithm that examines the data, selects the most appropriate statistical test, and analyzes the data accordingly.

The statistical analysis compares different data sets and checks for statistical significance. The data need to meet three criteria to be analyzed by a parametric test: independence, normality and variance homogeneity (Quinn and Keough, 2002). Fig. 8 presents a flow chart of the algorithm that is designed to check these three criteria and fit the most powerful statistical test to the data in order to reduce the probability that the results will be treated as not significant, even though they are (type II error).

In the first step (Fig. 8), the algorithm calculates the vector of medians. We use median and not mean because spike parameters are skewed to the right (Elhamdani et al., 2001; Wightman et al., 1991) and the median value from individual recordings gives a more robust representation of the population center (Mosharov and Sulzer, 2005; Sorensen et al., 2003). However, only cells with more than 20 spikes were chosen for analysis (Mosharov and Sulzer, 2005). Accordingly, for a specific tested spike parameter (e.g. spike amplitude), each cell contributes a single value (its median) to the analyzed data. This is done for two reasons. First, to make the different data sets independent as required for both parametric and nonparametric tests: each cell has its own spike characteristics, thus the measurements within each sample are dependent and

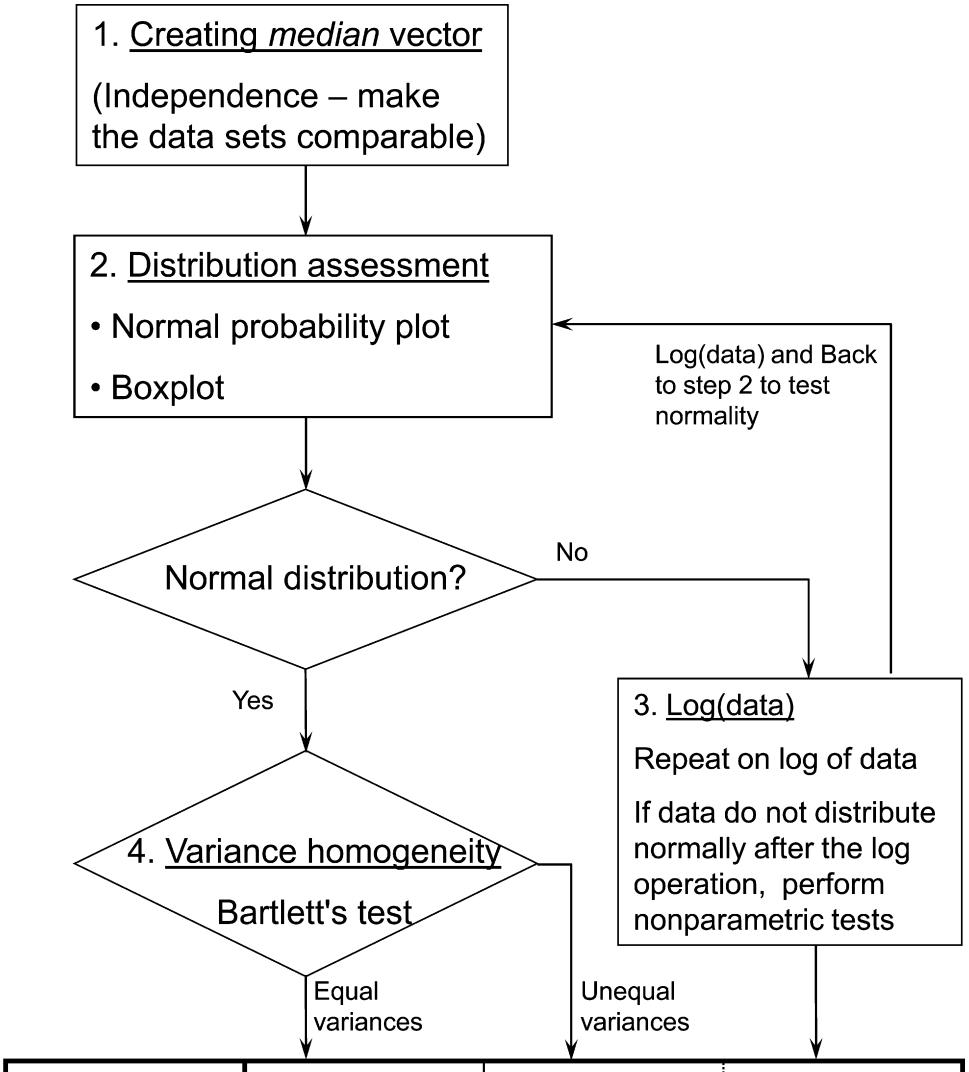

Fig. 8. Flow chart of the statistical analysis. See text for details.

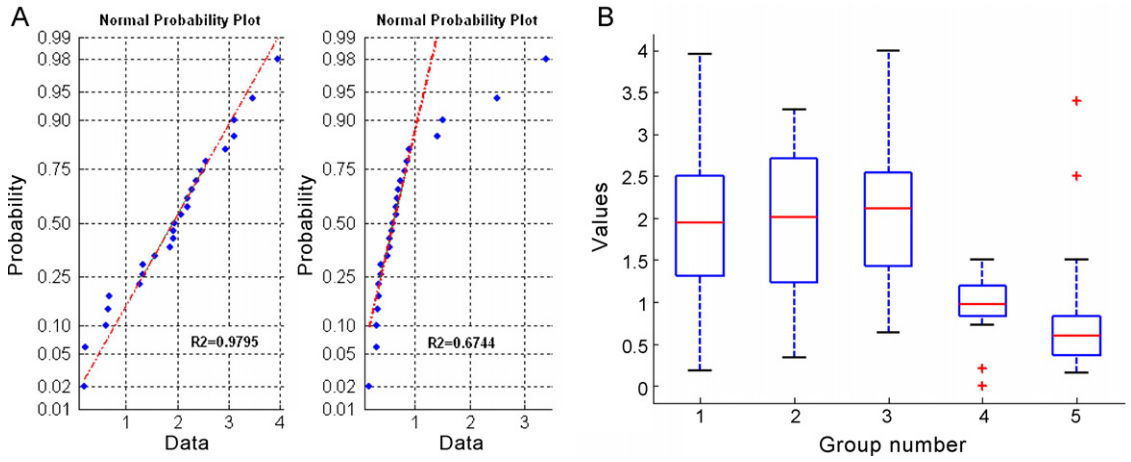

Fig. 9. Assessing normal distribution using graphical tools. (A) Normal probability plot. Left: normally distributed data. Right: skewed data. (B) Boxplot graph. The three left groups represent normally distributed data and the two right groups represent skewed distribution of data.

cannot be pooled into one random sample of the measured data (Colliver et al., 2000). Second, to give each cell the same weight in the total result: if the data are not weighted, a cell with many spikes will affect the mean more than a cell with fewer spikes and will shift the average results (Colliver et al., 2000). Although the number of spike events varies among different cells, no correlation has been found between the mean of spike characteristics and the number of events recorded from a cell (Colliver et al., 2000).

In the next step, the algorithm assesses whether the medians of each group distribute normally. The use of statistical tests to assess normality is problematic with a small number of samples, and a common alternative is therefore graphical assessment with a normal probability plot and boxplot (Quinn and Keough, 2002). The normal probability plot displays the median vector and a superimposed line (Fig. 9A) which joins the first and third quartiles of each column of the median vector (from 25% to 75%, Fig. 9A, red line). This line is extrapolated out to the ends of the sample to help evaluate the linearity of the data. When the data come from a normal distribution, the plot appears linear (Fig. 9A, left). When the data are not normally distributed (Fig. 9A, right), the data diverge significantly from the linear line. (For interpretation of the references to color in this text, the reader is referred to the web version of the article.)

To help the user assess the goodness of fit of the linear model to the data, the algorithm also provides the R^2 value. Data with R^2 higher than 0.95 are considered normally distributed. Based on our experiments and because of the robustness of the parametric tests used, we derived that R^2 higher than 0.9 is also acceptable. While a normal probability plot better suits a sample size of 25 or more, a boxplot (Fig. 9B) can be used from a sample size of 8 (Quinn and Keough, 2002). The box has lines at the first quartile (25%, blue), median (red), and upper quartile (75%, blue) values. Extreme values (red crosses) are data with values beyond the ends of the bars (MATLAB, 2004). When the data distribute normally, there are no extreme values and the box and bars are symmetrical on both sides of the median (Fig. 9B, groups 1–3). When the data are not normally distributed, the box graph is not symmetrical and there are extreme values, which are easily identified by the user (Fig. 9B, groups 4 and 5). Based on the boxplot, the normal probability plot and the R^2 values, the user evaluates whether the data are normally distributed.

If the medians from one/all of the groups do not distribute normally, we perform a log operation on the original data (Fig. 8, step 3). When the data include zero values, we determine the root mean square of the data, which is less effective, but more suitable. An advantage of the log operation is that it reduces the variance (Quinn and Keough, 2002), hence reducing the probability of false significance caused by a few extreme values. This approach is widely used, especially for the spike's charge and foot parameters (Amatore et al., 2005; Elhamdani et al., 2001; Mosharov and Sulzer, 2005). The rationalization for transforming data to different scales before data analysis is based in large part on acknowledging that the scales of measurement that we use are often arbitrary (Quinn and Keough, 2002). If the log/square vectors still do not distribute normally, we perform nonparametric hypothesis testing on the original median vectors. To compare the medians of two groups we use the Wilcoxon rank-sum test, which is equivalent to the Mann–Whitney *U* test (MATLAB, 2004). For three groups, we use the Kruskal–Wallis nonparametric one-way ANOVA (MATLAB, 2004) and the Dunn test post hoc (Giuseppe, 2007; Kirk, 1982).

If the median vectors or log vectors do distribute normally, we check the variance homogeneity assumption using Bartlett's test (Filliben and Heckert, 2007) (Fig. 8, step 4). If the variances of the two groups are equal, the algorithm performs a Student's *t*-test in the case of two groups (MATLAB, 2004; Sheskin, 1997), and one-way ANOVA (Kirk, 1982; MATLAB, 2004) in the case of three or more groups. To complete the analysis, the algorithm performs a Tukey–Kramer test post hoc (Sheskin, 1997). When the data are normally distributed but the variances are unequal, the algorithm uses the unequal *t*-test (MATLAB, 2004) to compare the means of two groups, the Welch procedure (Welch, 1951) for three groups and the Games–Howell procedure (Kirk, 1982) as a post hoc test.

3. Discussion

We developed a robust algorithm that identifies spikes and analyzes their parameters automatically. The idea for the spike-identification algorithm came from observing how humans identify spikes—first finding the spike's peak high above the noise level (crude threshold), then zooming in to find its start/end points (dynamic threshold) and finally, in the case of small spikes, comparing the result to an expected signal shape. The methods for amperometry analysis presented so far rely on filtering (Chow and von Rüden, 1995; Hof, 2003) and signal derivative for spike identification (Gomez et al., 2002; Mosharov, 2008; Mosharov and Sulzer, 2005). The motivation for developing this approach was (a) to avoid filtering—so that data would not be lost or distorted and (b) to have a fully automated algorithm which would accelerate the analysis and minimize human intervention to avoid possible subjectivity and would also include a built-in statistical analysis.

The shift-correction operation was originally considered a technical pre-processing step, but proved to be a significant milestone in

the spike identification. The importance of this step is that by having the noise oscillate around zero throughout the experiment, the entire data set can be used to calculate the most effective threshold and then the same threshold can be used throughout the whole experiment. The threshold is calculated after the shift correction by measuring the SNR of the entire data set, and dynamically evaluating the minimal threshold, keeping practically all noise peaks outside the calculations. The first iteration can be seen as a "first guess" threshold that is used for removing extreme outliers and calculating the s.d. The s.d. is used to calculate the preliminary SNR. Finally, refined high and low thresholds are calculated as a function of the SNR. This method can be seen as a classification algorithm which is designed to achieve maximal sensitivity by iteratively refining noise levels, to find a threshold that effectively separates noise peaks from signal peaks. Since we designed this method to find even the smallest signals, the algorithm had to effectively disqualify high-peak noise. This is achieved by automatically qualifying or disqualifying signal candidates based on their shape, thus maintaining a low threshold while avoiding false positives. These algorithms were successfully implemented on data sets from other labs (Feinshreiber et al., 2010; Fig. S1, Supplemental methods).

The duration of the linear phase is a significant parameter in the biological model and represents an index of the rate of catecholamine release (Fulop and Smith, 2007; Lindau and Alvarez de Toledo, 2003). The commonly used algorithm for fitting a spike's rising phase relies on fixed arbitrary numbers of the spike amplitude (30–70%, 35–65%, 50–90%), and these numbers are chosen to allow identification the rising phase in many spikes as possible (Chow and von Rüden, 1995; Fulop and Smith, 2007; Hof, 2003; Mosharov and Sulzer, 2005). Our algorithm checks for a string of consecutive increases, identifying the exact linear phase of each spike by fitting it to the R^2 model. This method takes as many points as possible for the linear fitting, improving the accuracy of the line fit. For example, in very quick spikes, the 30–70% method sometimes leaves only a few points; our method was able to use an extended range (e.g. 15–85%) that better describes the linear stage. Second, the new method is able to find a linear phase in spikes where the traditional method fails, for example, spikes that have a very big foot. The algorithm we present does not use two arbitrary numbers but rather iterates on the rising phase points to fit a linear equation based on the statistical model, identifying the full rising phase of the spike which represent the opening of the fusion pore (Fulop and Smith, 2007; Lindau and Alvarez de Toledo, 2003).

Automating the data analysis improves lab work in several respects. First, the algorithm for linear-phase fitting was successful in analyzing 9 out of 10 spikes, thus introducing a common basis for the experimental analysis by reducing the effect of subjectivity and human error inherent to manual analyses. Second, fully automated identification and analysis of the spikes makes the analytical process more efficient. Acceleration of this process allows the lab to focus on performing more biological experiments, which in turn increases the validity of the data. The efficiency stems not only from the automation, but also from gathering all of the analytical steps in a single platform. The program performs all tasks, from finding the spikes to performing the statistical analysis of the entire experiment.

The built-in statistical analysis is designed especially for the task of single-spike analysis. The use of a median vector reduces the probability of a type I error (false positive), which is more likely when grouping the whole spike population together. The correct use of statistical tests also reduces the probability of a type II error, where the use of an inappropriate statistical test may produce a false negative result.

The algorithms presented here can be used on different kinds of data sets as demonstrated in Fig. S2 (Supplemental methods). These principles can be implemented in all cases in which the noise has distinct statistical parameters (not necessarily normally distributed) that differ from those of the data. The main improvement of the algorithm over the analytical procedure is the use of a dynamic threshold to differentiate spikes from background noise without any filtration of the data.

Acknowledgments

We would like to thank Gil Friedrich for introducing us to MATLAB, Dr. Ilana Gelernterfor the statistical advice, Dr. Corey Smith for sharing his data with us and Dr. Anton Sheinin for his help with Igor. This work was supported by Israel Science Foundation Grant 1211/07 (U.A.).

Appendix A. Supplementary data

Supplementary data associated with this article can be found, in the online version, at doi:10.1016/j.jneumeth.2010.09.004.

References

Albillos A, Dernick G, Horstmann H, Almers W, Alvarez de Toledo G, Lindau M. The exocytotic event in chromaffin cells revealed by patch amperometry. Nature 1997;389:509–12.
Amatore C, Arbault S, Bonifas I, Bouret Y, Erard M, Ewing A, et al. Correlation between vesicle quantal size and fusion pore release in chromaffin cell exocytosis. Biophys J 2005;88:4411–20.
Amatore C, Arbault S, Bonifas I, Guille M. Quantitative investigations of amperometric spike feet suggest different controlling factors of the fusion pore in exocytosis at chromaffin cells. Biophys Chem 2009;143:124–31.
Borisovska M, Zhao Y, Tsytsyura Y, Glyvuk N, Takamori S, Matti U, et al. v-SNAREs control exocytosis of vesicles from priming to fusion. EMBO J 2005;24:2114–26.
Bruns D, Riedel D, Klingauf J, Jahn R. Quantal release of serotonin. Neuron 2000;28:205–20.
Burgoyne R, Barclay J. Splitting the quantum: regulation of quantal release during vesicle fusion. Trends Neurosci 2002;25:176–8.
Chow R, von Rüden L. Electrochemical detection of secretion from single cell. In: Sakmann B, Neher E, editors. Single-channel recording. New York and London: Plenum Press; 1995. p. 245–72.
Colliver T, Hess E, Pothos E, Sulzer D, Ewing A. Quantitative and statistical analysis of the shape of amperometric spikes recorded from two populations of cells. J Neurochem 2000;74:1086–97.
Elhamdani A, Palfrey H, Artalejo C. Quantal size is dependent on stimulation frequency and calcium entry in calf chromaffin cells. Neuron 2001;31:819–30.
Feinshreiber L, Singer-Lahat D, Friedrich R, Matti U, Sheinin A, Yizhar O, et al. Non-conducting function of the Kv2.1 channel recruits vesicles in neuroendocrine and nerve cells. J Cell Sci 2010;123:1940–7.
Filliben J, Heckert A.Croarkin C, Tobias P, editors. NIST/SEMATECH e-handbook of statistical methods; 2007.
Friedrich R, Groffen A, Connell E, van Weering J, Gutman O, Henis Y, et al. DOC2B acts as a calcium switch and enhances vesicle fusion. J Neurosci 2008;28:6794–806.
Fulop T, Smith C. Matching native electrical stimulation by graded chemical stimulation in isolated mouse adrenal chromaffin cells. J Neurosci Methods 2007;166:195–202.
Giuseppe C. Dunn's procedure for multiple, nonparametric, comparisons (m. file for MATLAB); 2007.
Gomez J, Brioso M, Machado J, Sanchez J, Borges R. New approaches for analysis of amperometrical recordings. Ann N Y Acad Sci 2002;971:647–54.
Hof D. AmperoStat. 2003: Igor macro.
Jankowski G, Schroeder T, Edward L, Wightman R. Temporal characteristics of quantal secretion of catecholamine from adrenal medullary cells. J Biol Chem 1993;268:14694–700.
Kirk R. Experimental design. 2nd ed Brooks/Cole Publishing Company. A Division of Wadsworth, Inc.; 1982.
Koh D. Carbon fiber amperometry in the study of ion channels and secretion. In: Stockand J, Shapiro M, editors. Methods in molecular biology. ion channels: methods and protocols. Totowa, NJ: Humana Press, Inc.; 2006.
Lindau M, Alvarez de Toledo G. The fusion pore. Biochim Biophys Acta 2003;1641:167–73.
Marom M, Hagalili Y, Sebag A, Tzvier L, Atlas D. Conformational changes induced in voltage-gated calcium channel Cav1.2 by BayK 8644 or FPL64176 modify the kinetics of secretion independently of Ca^{2+} influx. J Biol Chem 2010;285:6996–7005.
Marom M, Sebag A, Atlas D. Cations residing at the selectivity filter of the voltage-gated Ca^{2+}-channel modify fusion-pore kinetics. Channels (Austin) 2007;1:377–86.
MATLAB. MATLAB, Statistics Toolbox. The Mathworks, Inc; 2004.
Mosharov E. Analysis of single-vesicle exocytotic events recorded by amperometry. Methods Mol Biol 2008;440:315–27.

Mosharov E, Sulzer D. Analysis of exocytotic events recorded by amperometry. Nat Methods 2005;2:651–8.
Quinn G, Keough M. Experimental design and data analysis for biologists. Cambridge: The Press Syndicate of the University of Cambridge; 2002.
Segura F, Brioso M, Goĭmez J, Machado J, Borges R. Automatic analysis for amperometrical recordings of exocytosis. J Neurosci Methods 2000;103:151–6.
Sheskin D. Handbook of parametric and nonparametric statistical procedures. CRC Press; 1997.
Sorensen J, Nagy G, Varoqueaux F, Nehring R, Brose N, Wilson M, et al. Differential control of the releasable vesicle pools by SNAP-25 splice variants and SNAP-23. Cell 2003;114:75–86.
Welch B. On the comparision of several mean values: an alternative approach. Biometrika 1951;38:330–6.
Wightman R, Jankowski J, Kennedy R, Kawagoe K, Schroeder T, Leszczyszyn D, et al. Temporally resolved catecholamine spikes correspond to single vesicle release from individual chromaffin cells. Proc Natl Acad Sci USA 1991;88:10754–8.
Yizhar O, Matti U, Melamed R, Hagalili Y, Bruns D, Rettig J, et al. Tomosyn inhibits priming of large dense-core vesicles in a calcium-dependent manner. Proc Natl Acad Sci USA 2004;101:2578–83.
Zhang Z, Jackson M. Temperature dependence of fusion kinetics and fusion pores in Ca^{2+}-triggered exocytosis from PC12 cells. J Gen Physiol 2008;131:117–24.
Zhou Z, Misler S, Chow R. Rapid fluctuations in transmitter release from single vesicles in bovine adrenal chromaffin cells. Biophys J 1996;70:1543–52.